Relation between optical and chemical properties of dust aerosol over Beijing, China

Kan Huang,[1] Guoshun Zhuang,[1] Yanfen Lin,[1] Juan Li,[1] Yele Sun,[2] Wenjie Zhang,[3,4] and Joshua S. Fu[5]

Received 16 September 2009; revised 8 January 2010; accepted 31 March 2010; published 3 August 2010.

[1] Characteristics of optical and chemical properties of dust aerosol over Beijing and their relation were studied in the spring dust season, 2006 to understand the impact of dust and anthropogenic aerosol on the regional climate. Two dust plumes (DS1 and DS2) were identified with contrasting physicochemical properties. Strong absorbing of aerosol at 439 nm was observed, probably due to the significant proportion of iron oxides in the dust aerosol other than black carbon. The transport pathways of dust, concentrations of pollutant precursors and meteorological conditions were the main factors affecting the mixing extent of pollutants with dust. Aerosol of DS1 was more "polluted" than that of DS2 and even non-dust (ND) days. Pollution elements, i.e., Zn, As, Pb, S, and Cd, were greatly enriched in DS1; SO_4^{2-}, NO_3^-, NH_4^+, and K^+ significantly increased in dust storm episode, especially in DS1, indicating the strong heterogeneous chemical reaction occurred on dust and the mixing of dust with various pollutants during the long-range/regional transport of dust plumes. Linear relationship between optical properties and aerosol chemical composition was found. Soluble ions, i.e., SO_4^{2-}, NO_3^-, NH_4^+, and K^+, were the major contributors to the light extinction in fine particles, while mineral aerosol contributed more to that in coarse particles. Black carbon, as a strong light absorbing species, was found to contribute to the light extinction in both fine and coarse particles.

Citation: Huang, K., G. Zhuang, Y. Lin, J. Li, Y. Sun, W. Zhang, and J. S. Fu (2010), Relation between optical and chemical properties of dust aerosol over Beijing, China, *J. Geophys. Res.*, *115*, D00K16, doi:10.1029/2009JD013212.

1. Introduction

[2] East Asia is one of the most important pollution source regions over the world due to the rapid growth of economic development and population explosion. The atmosphere is now suffering from the mixed sources of anthropogenic aerosol related to the increased demand of fossil fuels and the natural aerosol such as dust aerosol originating from the northern/western dust source regions (Gobi Desert and Taklimakan Desert). Large field campaigns, such as Asian Pacific Regional Aerosol Characterization Experiment (ACE-Asia) [*Huebert et al.*, 2003] and Atmospheric Brown Cloud East Asian Regional Experiment 2005 (EAREX 2005) [*Nakajima et al.*, 2007] were conducted to investigate the physical, chemical, and optical properties of aerosol in northeast of Asia. Especially, the Aeolian Dust Experiment on Climate Impact (ADEC) was carried out to understand the impact of aeolian dust on climate via radiative forcing [*Mikami et al.*, 2006]. Beijing, the capital and megacity of China, has been facing the severe local anthropogenic pollution due to vehicle emissions/coal burning [*Sun et al.*, 2004] and the long-range transport of dust [*Sun et al.*, 2005; *Wang et al.*, 2005]. The mixing of dust with pollution aerosol has been observed by various approaches. During the peak dust season at eastern Asian sites, the monthly mean Angstrom exponent (440–870 nm) was observed to be even larger than 0.8, suggesting that fine mode pollution aerosol emitted from population centers in eastern Asia dominated even in spring as pollution aerosol mixes with coarse mode dust [*Eck et al.*, 2005]. Polarization lidar results showed the monthly averaged backscattering coefficients of dust near the surface were 0.003/km/sr in Beijing, 0.001–0.002/km/sr in Nagasaki, and 0.0006/km/sr in Tsukuba, respectively, indicating the internal mixing of mineral dust and anthropogenic aerosols [*Shimizu et al.*, 2004]. Analysis of individual Asian dust storm particles indicated that about one fifth of all the particles were mineral aggregates, while at least one fourth of the particles contained sulfur [*Shi et al.*, 2005] and *Yuan et al.* [2004] suggested the major form of sulfur were $CaSO_4$ and $(NH_4)_xH_{2-x}SO_4$, which mixed with the quartz and clay. It is believed that dust particles had mixed well with pollution

[1]Center for Atmospheric Chemistry Study, Department of Environmental Science and Engineering, Fudan University, Shanghai, China.
[2]Department of Environmental Toxicology, University of California, Davis, California, USA.
[3]Center for Atmospheric Environmental Study, Department of Chemistry, Beijing Normal University, Beijing, China.
[4]Chinese Research Academy of Environmental Sciences, Beijing, China.
[5]Department of Civil and Environmental Engineering, University of Tennessee, Knoxville, Tennessee, USA.

0148-0227/10/2009JD013212

substances during the transport [*Guo et al.*, 2004]. The airborne calcium carbonate (calcite), an important fugitive dust constituent, could react with sulfuric acid aerosols from industrial sources to form two hydrated forms of calcium sulfate [*Davis and Jixiang*, 2000]. The secondary sulfate/nitrate and total pollutants could have contributed 25% and 40–50%, respectively, to the total suspended particles in the dust episodes [*Yuan et al.*, 2008].

[3] Beijing had been influenced by several dust events during the spring season in 2006. A synergy of Lidar, Sun photometric and satellite measurements were applied to depict this extraordinary dust event over Beijing [*Papayannis et al.*, 2007]. Aircraft measurements during this period investigated the vertical distribution and size distribution of the ultrafine particles during the dust storm and non-dust storm periods [*Wang et al.*, 2008]. The mineralogy and magnetic properties of the dust storm samples collected on 17 and 18 April, 2006 were studied, which indicated that the dust might be mixed with anthropogenic particles during the transport [*Feng et al.*, 2008; *Zheng and Zhang*, 2008]. Besides, *Sun and Zhao* [2008] simulated the dust emission, transport, and deposition of the two severest dust storm events. However, no investigation of optical and chemical properties of this spring dust storm could be found anywhere in current literature. In this study, we will focus on the aerosol optical and chemical properties of the two dust plumes in spring 2006 and try to link the aerosol optical properties with its chemical compositions.

2. Experiments and Methods

2.1. Sampling

[4] Aerosol samples of TSP and $PM_{2.5}$ were collected daily in Beijing from March to April in the spring of 2006, using medium-volume samplers manufactured by Beijing Geological Instrument-Dickel Co., Ltd. (model: TSP/PM_{10}/$PM_{2.5}$-2; flow rate: 77.59 L/min). All the samples were collected on the roof (~40 m) of the Building of Science & Technology in Beijing Normal University using Whatman® 41 filters (Whatman Inc., Maidstone, UK). The duration time of sampling was generally 24 h. More samples with shorter duration time were collected during the dust days in order to better characterize the dust. The filters before and after sampling were weighed using an analytical balance (Model: Sartorius 2004MP) with a reading precision 10 mg after stabilizing under constant temperature (20 ± 1°C) and humidity (40 ± 1%). All the procedures were strictly quality controlled to avoid the possible contamination of the samples.

2.2. Chemical Analysis

2.2.1. Ion Analysis

[5] One-fourth of each sample and blank filter was extracted ultrasonically by 10 mL deionized water (18MΩcm^{-1}). Eleven inorganic ions (SO_4^{2-}, NO_3^-, F^-, Cl^-, NO_2^-, PO_4^{3-}, NH_4^+, Na^+, K^+, Ca^{2+}, Mg^{2+}) and four organic acids (formic, acetic, oxalic, and methylsulfonic acid (MSA)) were analyzed by Ion Chromatography (IC, Dionex 600), which consists of a separation column (Dionex Ionpac AS 11), a guard column (Dionex Ionpac AG 11), a self-regenerating suppressed conductivity detector (Dionex Ionpac ED50) and a gradient pump (Dionex Ionpac GP50). The detail procedures were given elsewhere [*Yuan et al.*, 2003].

2.2.2. Element Analysis

[6] Half of the sample filters were digested at 170°C for 4 h in high-pressure Teflon digestion vessel with 3 ml concentrated HNO_3, 1 ml concentrated HCl, and 1 ml concentrated HF. After cooling, the solutions were dried, and then diluted to 10 ml with distilled deionized water. Total 19 elements (Al, Fe, Mn, Mg, Ti, Sc, Na, Sr, Ca, Co, Cr, Ni, Cu, Pb, Zn, Cd, V, S, and As) were determined by inductively coupled plasma atomic emission spectroscopy (ICP-AES; Model: ULTIMA, JOBIN-YVON Company, France). The detailed analytical procedures were given elsewhere [*Sun et al.*, 2004; *Zhuang et al.*, 2001].

2.2.3. Black Carbon Analysis

[7] Black carbon (BC) was analyzed with Smokerstain Reflectometer (UK, Model, M43D) on Whatman® 41 filters.

2.3. AERONET Ground Observations

[8] Aerosol optical properties were collected from the Aerosol Robotic Network (AERONET) performed by a Sun/Photometer located in Beijing [*Holben et al.*, 1998]. The bandwidth of each channel is 10 nm. Various parameters of aerosol optical properties were retrieved at 440 nm, 670 nm, 870 nm, and 1020 nm. Aerosol size distribution, refractive index, and single-scattering albedo can be retrieved by using sky radiance almucantar measurements and direct sun measurements [*Dubovik and King*, 2000]. The accuracy of the presented AOD measurements is of the order of ± 0.03 regarding the level 1.5 (cloud-screened) data.

2.4. Meteorological Data

[9] The meteorological data, including temperature, dew point, relative humidity, wind speed, wind direction and visibility were collected from http://www.wunderground.com. Air pollution index (API, API = 100 corresponds to Chinese air quality standard II) of SO_2 and NO_2 in Beijing during the sampling period was collected from http://www.bjee.org.cn, the API were converted to the mass concentrations using the following formula:

$$C = C_{low} + [(I - I_{low})/(I_{high} - I_{low})] \times (C_{high} - C_{low})$$

where C is the concentration and I is the API value. I_{high} and I_{low}, the two values most approaching to value I in the API grading limited value table, stand for the value higher and lower one than I, respectively; C_{high} and C_{low} represent the concentrations corresponding to I_{high} and I_{low}, respectively.

3. Results and Discussion

3.1. Monitoring and Source Identification of Two Dust Plumes

[10] Figure 1 shows the temporal variations of mass concentrations of $PM_{2.5}$ and TSP from March 28th to April 28th in Beijing, 2006. During this period, the concentrations of both fine and coarse particles fluctuated greatly, reflecting possible contributions from miscellaneous sources, atmospheric processing or transport pathways. Two big dust plumes were identified, one from April 8th to 11th and the other from April 17th to 18th, which were marked as DS1 and DS2 in Figure 1. These two dust plumes had also been monitored by the aircraft observation in Tianjin, which is nearby Beijing. DS1 was identified as a relatively small scale

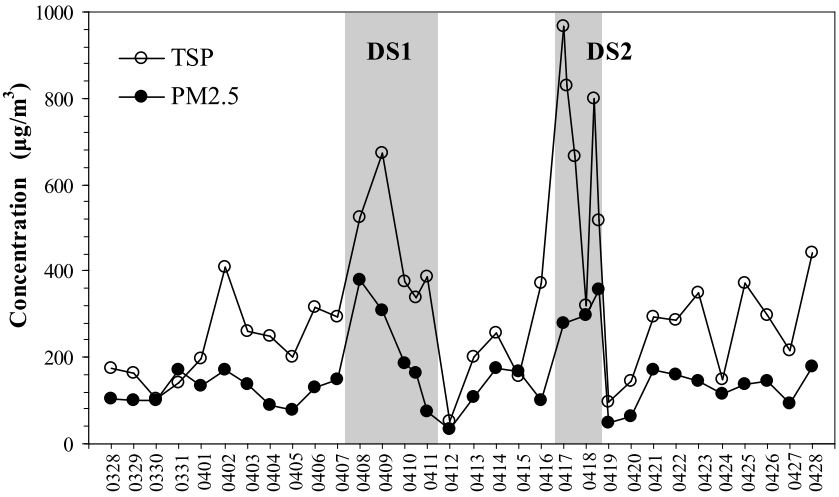

Figure 1. Temporal variations of mass concentrations of $PM_{2.5}$ and TSP in Beijing, 2006; two dust plumes (DS1, DS2) are marked as gray columns.

dust storm [*Wang et al.*, 2008], while DS2 was an intense one [*Papayannis et al.*, 2007; *Wang et al.*, 2008], which had influenced Korea [*Lee and Cho*, 2007] and even took the trans-Pacific transport to North America [*McKendry et al.*, 2008]. MODIS satellite captured these two dust plumes from the sky on April 10th and 17th (Figure 2) and both images showed the thick aerosol plumes obscuring over northeastern China and Bohai Bay. Obviously, DS2 was thicker and influenced larger area than DS1. The daily mass concentration of $PM_{2.5}$ and TSP during DS1 ranged from 75.2 to 377.5 and 355.0–672.1 $\mu g/m^3$ with the mean values of 222.1 and 459.2 $\mu g/m^3$, respectively. DS2 was more intense with the mean values of 310.9 and 683.3 $\mu g/m^3$ for $PM_{2.5}$ and TSP, respectively. Compared to the non-dust period (ND), which is defined as the remaining sampling days excluding DS1 and DS2, the aerosol concentrations during the dust periods were elevated about 2~3 times, probably indicating the entrainment of dust via the transport.

[11] Figure 3 shows the meteorological parameters of interest and the daily trace gas concentrations of SO_2 and NO_2 during the study period. The temperature didn't fluctuate greatly, while the dew point and relative humidity had significant variations and both reached very low values one or two days before the dust plumes, indicating the advent of cold fronts. Surprisingly, the average relatively humidity during the two dust plumes had an increase to a moderate value of nearly 60% (Table 1), which was quite different from the previous dust storms that happened over Beijing in 2001, 2002 and 2004 [*Wang et al.*, 2005, 2007; *Yuan et al.*, 2008], as the days when dust storms occurred were usually accompanied with low water content in the air. The moderate/high relative humidity could facilitate the chemical reactions on the dust particles and secondary aerosol formation would be favored due to the mixing of dust and pollutant precursors. Additionally, we found the wind speeds were relatively low (2.2~2.5 m/s) during the dust periods (Table 1), which was also different from the usual dust storms, in which the wind speeds were often high. *Feng et al.* [2008] also observed that the near-surface wind speed was insignificant during the dust storm and concluded that the

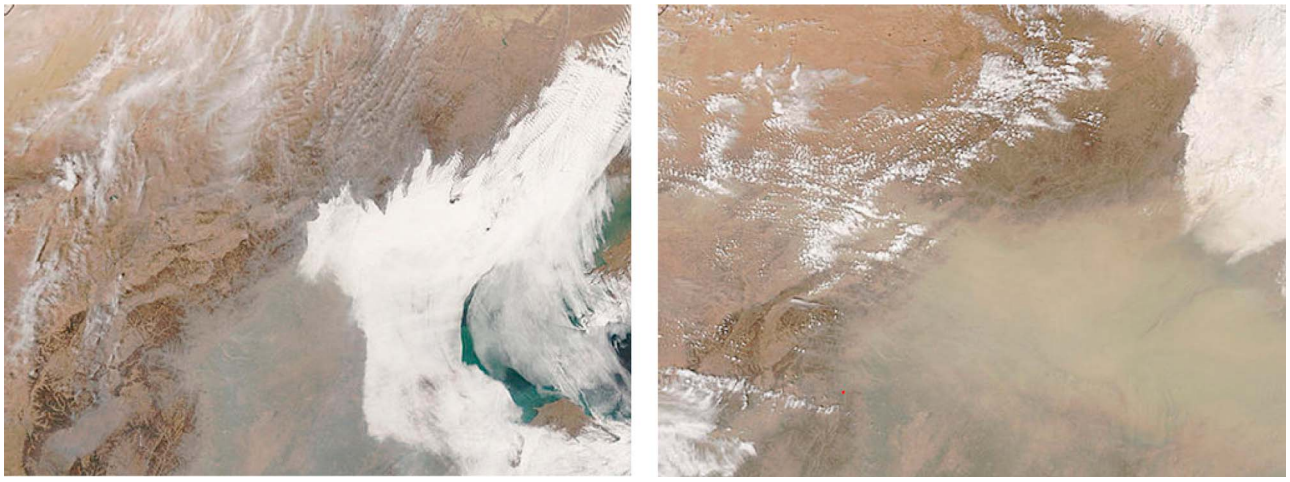

Figure 2. MODIS true color satellite images on (left) April 10th and (right) April 17th.

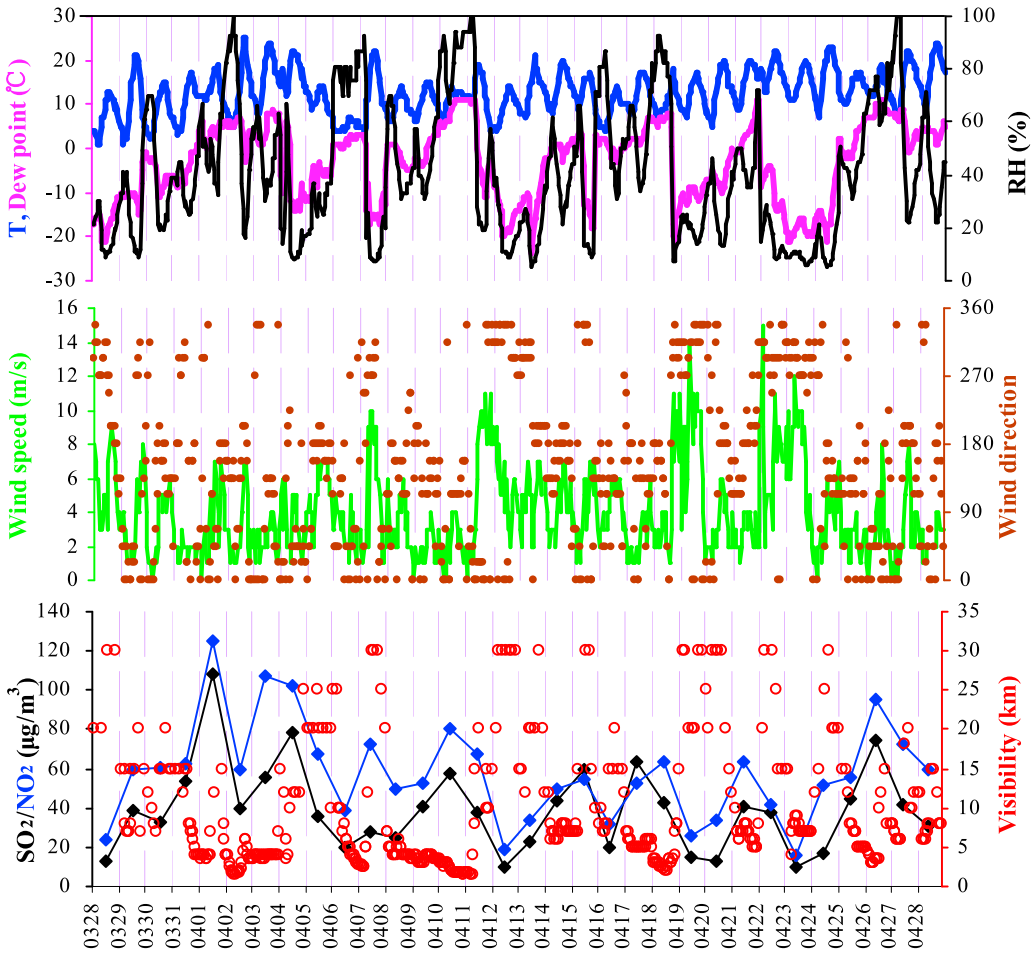

Figure 3. The meteorological parameters including temperature, dew point, relative humidity, wind speed, wind direction and visibility with daily trace gas concentrations of SO_2 and NO_2 during the study period.

dust should be mainly transported by upper northwestern winds and local dust of Beijing contributed little. Stagnant atmosphere would be caused by the relatively low wind speeds and this wasn't beneficial for the diffusion of dust/pollutants. Temporal variations of SO_2, NO_2, and visibility are also shown in Figure 3. SO_2 and NO_2 varied negatively with the visibility under most circumstances, indicating the effect of the gas-to-particle chemistry on the visibility. There were three low visibility periods, the first occurred from April 1st to 3rd with visibility lower than 5 km at most time. During this period, the daily concentration of SO_2 and NO_2 peaked at 108 and 125 $\mu g/m^3$, which was at the similar concentration level of the heavy haze that happened over Shanghai on January 19th, 2007, when the daily concentration of SO_2 and NO_2 reached 194 and 123 $\mu g/m^3$ [*Fu et al.*, 2008], respectively, indicating the low visibility was caused by the local photochemistry. The other two low visibility periods occurred just during the two dust plumes and the low visibility of 4 km (Table 1) should be attributed to the high dust loadings. However, the trace gas concentrations were also high with mean values of 40.5 and 62.6 $\mu g/m^3$ for SO_2 and NO_2 in DS1, and 53.4 and 58.2 $\mu g/m^3$ in DS2 compared with those of 35.3 and 52.9 $\mu g/m^3$ in ND, respectively. This maybe suggested that the secondary aerosol formation from the gas-to-particle process could also contribute to the light extinction and the visibility degradation, although this effect was probably covered by the high concentrations of mineral dust. Aircraft measurements also observed the hazy weather around Beijing on April 9th [*Wang et al.*, 2008]. The cause of high pollution gas concentrations during the dust plumes was ambiguous and may be caused by the enhanced local source strength or regional transport and the unfavorable atmospheric conditions, e.g., low wind speed and moderate/high relative humidity.

[12] The backward air trajectory analysis using HYSPLIT4 (Hybrid Single-Particle Lagrangian Integrated Trajectory) Model from the NOAA/Air Resources Laboratory indicated two dust plumes both originated from the Gobi Desert in

Table 1. Mean Values of Meteorological Parameters During Non-dust Days and Two Dust Plume Periods[a]

	Temperature (°C)	Dew Point (°C)	RH (%)	Pressure (hPa)	Visibility (km)	Wind Speed (m/s)
ND	12.1	−4.6	38	1013	6.1	3.6
DS1	10.5	1.3	57	1011	4.0	2.2
DS2	12.0	0.5	59	1009	4.5	2.5

[a]ND, non-dust days; DS1 and DS2, dust plume periods.

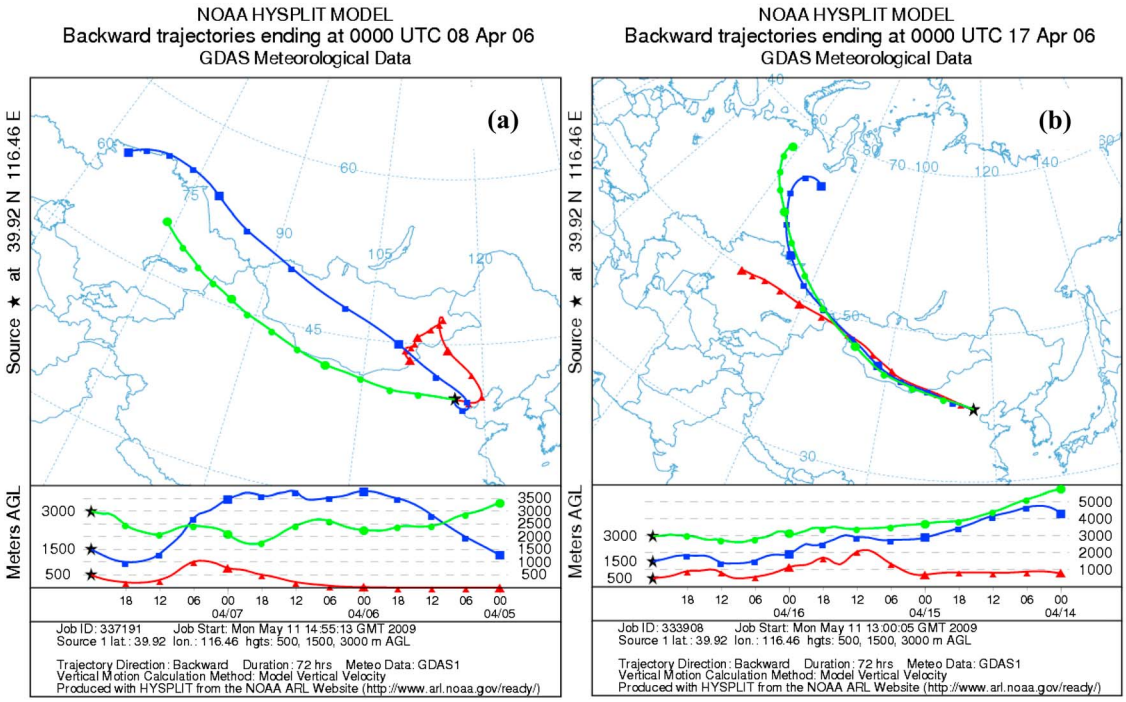

Figure 4. Air parcel 72-h backward trajectory ended at (a) April 8th (DS1) and (b) April 17th (DS2).

Mongolia and inner-Mongolia (Figure 4), which was also confirmed by the model simulation [*Papayannis et al.*, 2007] and the INTEX-B (Intercontinental Chemical Transport Experiment - Phase B) campaign [*McKendry et al.*, 2008]. The elemental ratio of Ca/Al also can be used to characterize the sources of the Asian dust [*Yuan et al.*, 2008] and we found that DS1 and DS2 had the similar ratios of 0.91 and 0.87, respectively, close to the northwestern Gobi dust source of 1.09 ± 0.13 [*Huang et al.*, 2010]. Anyway, the backward air trajectory results of the two dust plumes at the arrival heights of 500 m (within the PBL) indicated two different airflow movement patterns (Figure 4). In DS2, the airflow moved from the northwestern, as the nearly identical moving direction as the air masses at heights of 1500 m and 3000 m, while in DS1 it moved from the northeastern China (Figure 4b), where great population and heavy industries located there. Figure 5 shows the MODIS rapid response system fire map of northeastern China during the period of DS1, and we found there were large numbers of red fire hot spots in this region. As rich forests were planted there, this maybe suggested that the air masses of DS1 at the height of 500 m within the PBL could be influenced by the smoke aerosol that originated from the biomass burning. The different transport pathways of dust would probably have different impacts on the mixing of dust with pollutants and the aerosol chemistry.

3.2. Characteristics of the Two Dust Plumes

3.2.1. Optical Properties

[13] Aerosol optical depth (AOD) is a good indication of the airborne aerosol loading in the atmospheric column. The average values of AOD during ND, DS1 and DS2 at 440, 675, 870 and 1020 nm are shown in Figure 6a. AOD showed moderate values of 1.05 ± 0.71 in ND at 440 nm, but it was elevated several times during the dust plumes. The observed maxima of AOD reached 2.22 in DS1 (April 11th) and 3.65 in DS2 (April 17th), respectively. The appearance of the extremely high AOD should be mainly due to the entrainment of dust. For Dust AOD varies very little with wavelength [*Myhre et al.*, 2008], thus, the observed strong dependence of AOD on wavelength in this study would indicate the different size distribution of chemical species in aerosol.

[14] Figure 6b shows the scatterplot between AOD at 440 nm and Angstrom exponent (α) (440–870 nm). Angstrom exponent is a good indicator of the aerosol size

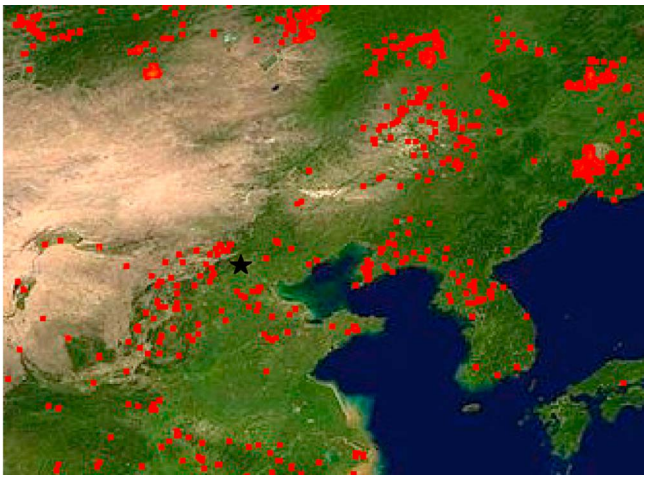

Figure 5. MODIS rapid response system fire map of northeastern China during the period of DS1 (the red dots represent the fire spots and the black star represents the observation site).

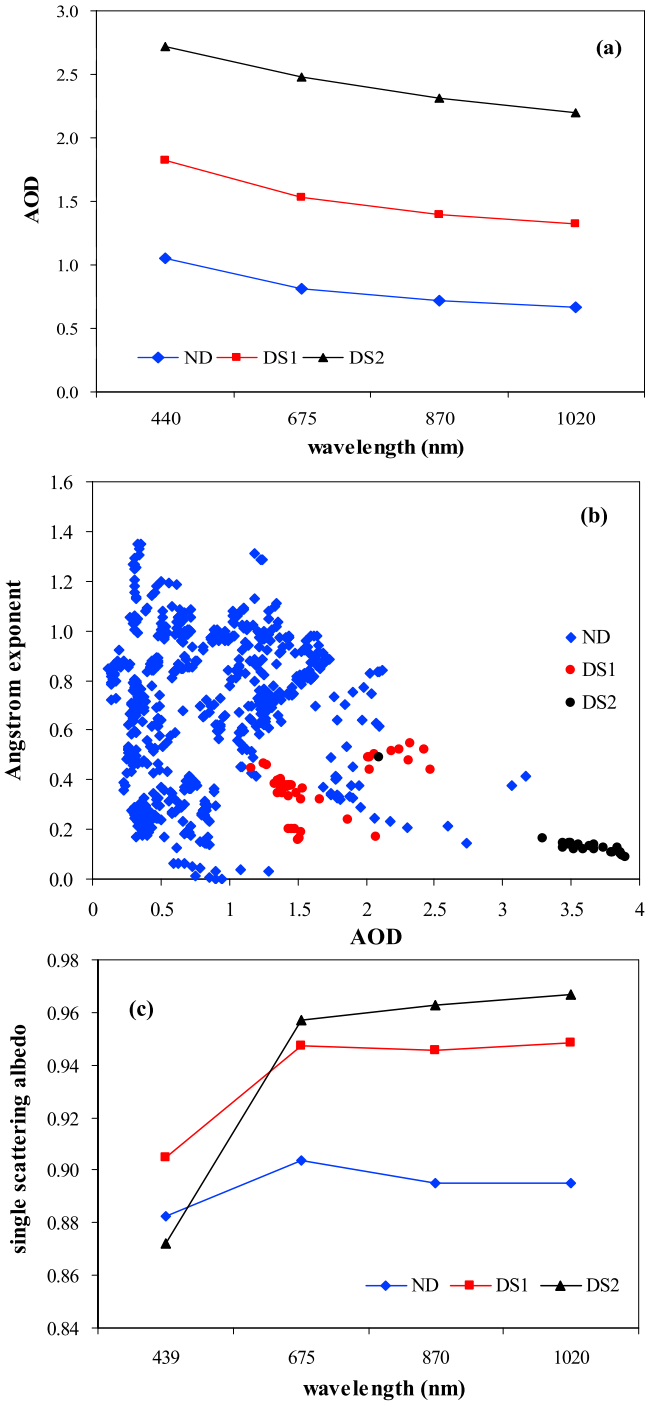

Figure 6. Aerosol optical properties in ND, DS1 and DS2. (a) The dependence of aerosol optical depth (AOD) on wavelength. (b) The relationship between Angstrom exponent and AOD. (c) The dependence of single scattering albedo on wavelength.

distribution, the larger the Angstrom exponent, the smaller the particle size, and vice versa. In ND, the dots distributed in a wide range, of which the high AOD with the high α values probably indicated the occurrence of haze days, which was characterized by high aerosol concentration and large fraction of fine particles. The low AOD with low α values maybe indicated the relatively clean days. The average AOD fine mode fraction (FMF) derived from the AERONET Sun/Sky photometer measurement in ND was at the moderate level of 0.40, indicating the fine particle pollution in non-dust days in Beijing. As for DS2, most of the dots were in the range of AOD > 3.0 and α < 0.2 and the average FMF value was as low as 0.18, indicating the presence of high aerosol loadings and very large particles. Compared to DS2, DS1 had relatively lower AOD and higher α values. As the intensity of DS1 was weaker than DS2, the lower AOD was expected. While the average FMF was 0.31, much higher than that of DS2, indicating the relatively stronger atmospheric processes in DS1 than in DS2.

[15] Figure 6c shows the average values of single scattering albedo (SSA) at four wavelengths during ND, DS1, and DS2, respectively. SSA is defined as the ratio of the aerosol scattering coefficient to the extinction coefficient (sum of the absorption and scattering coefficient) and is one of the main parameters determining the climatic effect of aerosol. The single scattering albedo was 0.90 ± 0.33 at 675 nm during ND in this study. Previous studies found similar results of 0.88 ± 0.44 at 500 nm in spring 2001 in Beijing [*Xia et al.*, 2005] and 0.88 ± 0.03 at 550 nm in Yellow Sea, Gosan during the dust season [*Anderson et al.*, 2003]. Compared to the SSA value of 0.98 in the dust source regions in China [*Xia et al.*, 2005], DS2 (0.96) was more close to it than DS1 (0.94). It was reported that SSA observed in Gwangju, Korea of the aerosol derived from Siberian forest fire was 0.94 ± 0.01 [*Noh et al.*, 2009] and the SSA observed in Tokyo, Japan of the aerosol derived from the similar source was 0.95 ± 0.06 [*Murayama et al.*, 2004]. The similar results of DS1 in this study supported the assumption that smoke aerosol had mixed with dust during the transport, which was based on the backward trajectory analysis and satellite images of fire spots.

[16] The spectral variation of aerosol SSA is determined by the chemical composition and microphysical properties [*Liu et al.*, 2008]. Decreasing SSA as a function of wavelength would indicate the mixing of dust with black carbon and organic matters [*Bergstrom et al.*, 2003; *Dubovik et al.*, 2002; *Kirchstetter et al.*, 2004] because of the stronger decrease with wavelength of the scattering coefficient than the absorption coefficient [*Alfaro et al.*, 2004], while the increasing SSA as a function of wavelength would indicate the dominance of the dust aerosol [*Dubovik et al.*, 2002] because of the larger imaginary refractive index of mineral dust at the short end of the solar spectrum [*Alfaro et al.*, 2004]. In this study, the dependence of SSA on wavelength didn't merely follow an increasing or decreasing trend. Apart from the 439 nm wavelength, the SSA of DS2 had a moderate increasing trend with wavelength from 675 to 1020 nm, similar to that observed by *Xia et al.* [2006] during the dust periods, indicating the dust input. On the contrary, the spectral dependence of SSA during ND exhibited a decreasing trend and no obvious dependence of SSA on wavelength was observed during DS1, which would indicate the mixing of dust with pollutant aerosol in ND and DS1 to some extent. At wavelength of 675, 870, and 1020 nm, SSA followed the order of DS2 > DS1 > ND, which indicated that dust SSA was generally larger than that of anthropogenic aerosols [*Xia et al.*, 2005]. Black carbon (BC) was the major light-absorbing component in aerosol in the visible and near-infrared wave-

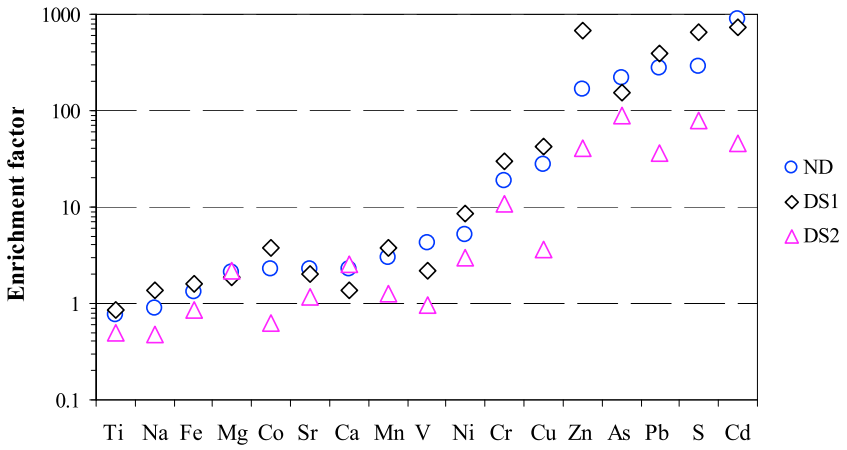

Figure 7. The average enrichment factors of major elements in $PM_{2.5}$ during ND, DS1 and DS2.

length. In ND, the average mass fraction of BC in $PM_{2.5}$ was (3.1 ± 1.0)%, higher than that of (2.4 ± 0.78)% and (1.2 ± 0.41)% in DS1 and DS2, respectively. As a result, higher aerosol absorption and lower SSA would be expected in the non-dust days than in the dust days. The results of the SSA values at 439 nm were much lower than those at the longer wavelengths and the SSA of DS2 at 439 nm was 0.87. even lower than that of ND and DS1, which indicated the strong light absorbing at 439 nm during the intense dust storm, although black carbon contributed lowest to the aerosol in DS2 as indicated above. The strong light-absorbing at wavelength of 439 nm could be explained by the influence of iron-oxide minerals on the reflectance spectra of aerosol, as hematite and goethite has pronounced absorbing peaks at 555 and 435 nm, respectively [*Arimoto et al.*, 2002; *Deaton and Balsam*, 1991]. We used the percentage of elemental Fe in TSP to evaluate the effect of iron-oxide minerals on the absorbing of aerosol, and found the average Fe/TSP value was (4.0 ± 1.5)% in DS2, which was the highest compared with that in ND and DS1 of (3.5 ± 1.4)% and (3.3 ± 0.8)%, respectively. This could explain the much lower SSA values in DS2 than ND and DS1 at 439 nm, for the effect of iron-oxide minerals on the light absorbing coefficient of aerosol contributed to the decrease of SSA, which was especially obvious during the high dust storm periods. *Raut et al.* [2009] also found that the high absorption properties of aerosol in the underground railway station were linked to the significant proportion of iron oxides together with black carbon in the braking system.

[17] *Che et al.* [2008] concluded that the significant differences of aerosol optical properties under background, haze, and dust days over Beijing was due to different aerosol components under distinct weather conditions. The chemistry of aerosols, the mixture state of aerosols components may account for large changes in ambient extinction, the portioning of scattering and absorption efficiency (SSA) and AOD relationship to water vapor [*Xia et al.*, 2007]. In the next section the chemical characteristics of aerosol in different conditions are compared to better elucidate the mixing process of mineral dust with pollution aerosol.

3.2.2. Chemical Properties

[18] The enrichment factor (EF) analysis can be used to evaluate the enrichment degree of the elements in the aerosol sample. Enrichment factor is defined as the ratio of the abundance of a particular element in aerosol to its abundance in the crust. Usually Al is used as the reference element for mineral source and the formula is calculated as $EF_x = (X/Al)_{aerosol}/(X/Al)_{crust}$, of which X is the element of interest. Species with EFs less than 10 usually have a major mineral source, while species with high EFs probably have a significant anthropogenic source. The average EF values of the measured 17 elements in $PM_{2.5}$ during ND, DS1 and DS2 are shown in Figure 7. These elements can be categorized into three groups. The first group, which included Ti, Na, Fe, Mg, Co, Sr, Ca, Mn, V, and Ni, had EFs lower than 10, indicating these elements were little contaminated and mainly derived from the mineral sources. The second group, which included Cr and Cu, had EFs of 10~100, indicating they were moderately contaminated and probably derived from the industrial emission and metallurgical furnace. For the last group consisted of Zn, As, Pb, S, and Cd, the EFs were 100~1000 and they mainly came from the anthropogenic sources such as coal combustion, vehicle/industry emissions, etc. We noticed that the EFs of the pollution elements generally followed the order of DS1 > ND > DS2, which suggested that DS1 was a more "polluted" dust plume while DS2 was relatively clean and this should be related much to the transport pathways of dust. As indicated above, anthropogenic pollutants and smoke aerosol could have been transported and mixed with dust when the air masses of DS1 moved from some industrial and urban regions to the observation site. This could explain why the pollution elements during DS1 were much more enriched.

[19] Table 2 summarizes the average ionic concentrations of TSP in ND, DS1, and DS2. Na^+, Mg^{2+}, and Ca^{2+}, which represented the mineral source, followed the order of DS2 > DS1 > ND. The mean concentrations of Na^+, Mg^{2+}, and Ca^{2+} in DS1 were 1.42, 0.81, and 7.77 $\mu g/m^3$, respectively, which was almost twice of that in ND. While in DS2, they were 2.48, 0.87, and 11.38 $\mu g/m^3$, the three times of that in ND. This was consistent with the aerosol loadings in the three different conditions, as DS2 contributed more mineral aerosols than DS1 and ND. In respect of the other ions, their mass concentrations followed the different order of DS1 > DS2 > ND (Table 2). The average sulfate concentrations in DS1 and DS2 were 29.65 and 20.55 $\mu g/m^3$, respectively,

Table 2. Average Concentrations of Soluble Ions in TSP During ND, DS1 and DS2[a]

Species	ND	DS1	DS2
F^-	0.35 (0.24)	0.56 (0.30)	0.36 (0.24)
CH_3COO^-	0.06 (0.12)	BDL	BDL
$HCOO^-$	0.004 (0.015)	0.019 (0.020)	BDL
Cl^-	2.84 (1.77)	5.46 (3.28)	4.81 (2.06)
NO_2^-	0.022 (0.027)	0.034 (0.031)	0.012 (0.029)
NO_3^-	8.32 (7.21)	15.26 (10.84)	8.64 (4.59)
SO_4^{2-}	9.98 (8.59)	29.65 (23.23)	20.55 (9.94)
$C_2O_4^{2-}$	0.22 (0.10)	0.39 (0.15)	0.27 (0.32)
Na^+	0.82 (0.44)	1.42 (0.70)	2.48 (0.99)
NH_4^+	1.98 (1.60)	4.36 (3.36)	2.99 (1.78)
K^+	1.11 (0.80)	2.94 (1.83)	1.35 (0.76)
Mg^{2+}	0.38 (0.18)	0.81 (0.33)	0.87 (0.32)
Ca^{2+}	4.68 (1.61)	7.77 (2.67)	11.38 (4.40)

[a]One standard deviation given in parentheses. BDL: below detection limit. Units: $\mu g/m^3$.

which were elevated about three and two times compared to that in ND. Mass percentages of 6.46% and 3.01% in DS1 and DS2, respectively, of sulfate in aerosol were much higher than that in the surface soils of 0.01% [*Nishikawa et al.*, 1991]. The elevated sulfate concentrations could be derived from the heterogeneous reaction of gaseous SO_2 on the mineral dust or the mixing of sulfate aerosol with mineral dust on the pathway. It was found that the mass percentage of sulfate in DS1 was much higher than DS2 and ND (4.19%), indicated the strong mixing of pollutants with dust in DS1. As for NO_3^- and NH_4^+, they increased about twice in DS1 while varied little in DS2 compared to that in ND (Table 2). The increase of nitrate and ammonium in DS1 was probably due to the more "polluted" dust transport pathway as mentioned above. While in DS2, the relatively low concentrations of NO_3^- and NH_4^+ suggested the dilution effect by the dust, for the intensity of DS2 was much stronger than DS1. K^+ is used as the tracer of the biomass burning source. The average concentration of K^+ in ND, DS1, and DS2 was 1.11, 2.94, and 1.35 $\mu g/m^3$, respectively, reflecting the enhancement of smoke aerosol during DS1, which was also consistent with the backward trajectory analysis and MODIS fire spot images, as shown in Section 3.1. Chloride was also elevated during the two dust plumes. Cl^- could derive from the waste incineration as well as coal burning. The elevated Cl^- could also come from the saline minerals of dried salt lakes or saline soils in northern China [*Yuan et al.*, 2006] when the dust plumes passed over these regions. In addition to the secondary inorganic ions, the organic acids such as CH_3COO^-, $HCOO^-$ and $C_2O_4^{2-}$ also increased in DS1 (Table 2), indicating the enhanced photochemical production of secondary organic aerosol in DS1. As a whole, the total water soluble ions contributed an average mass percentage of 12%, 17%, and 9% to aerosol in ND, DS1, and DS2, respectively. These results confirmed the pollution nature of DS1, which was consistent with the element analysis mentioned above.

[20] Relationship between acids (SO_4^{2-}, NO_3^-) and bases (NH_4^+, Ca^{2+}) could shed some light on the chemical transformation processes during the transport of dust as these ions were the major contributors to the soluble ions. SO_4^{2-} and NO_3^- both had strong correlations with NH_4^+ with the correlation coefficients of 0.97 and 0.91 during the whole sampling period, respectively. Figure 8a shows the correlation of the equivalent concentrations of NH_4^+ with the sum of the equivalent concentrations of SO_4^{2-} and NO_3^- in TSP. Distinguished by different colors, NH_4^+ almost acted the similar neutralization role on the acids in non-dust days or dust plume days. The correlation coefficient between the two variables was as high as 0.98 for all the dots. This indicated that dust almost had no influence on the neutralization ability of NH_4^+. Anyway, the slope of the regression was only 0.30, much lower than the unity, which meant 70% of the total acids hadn't been neutralized by NH_4^+. In the northern China, the dust aerosol contained a considerable fraction of calcium

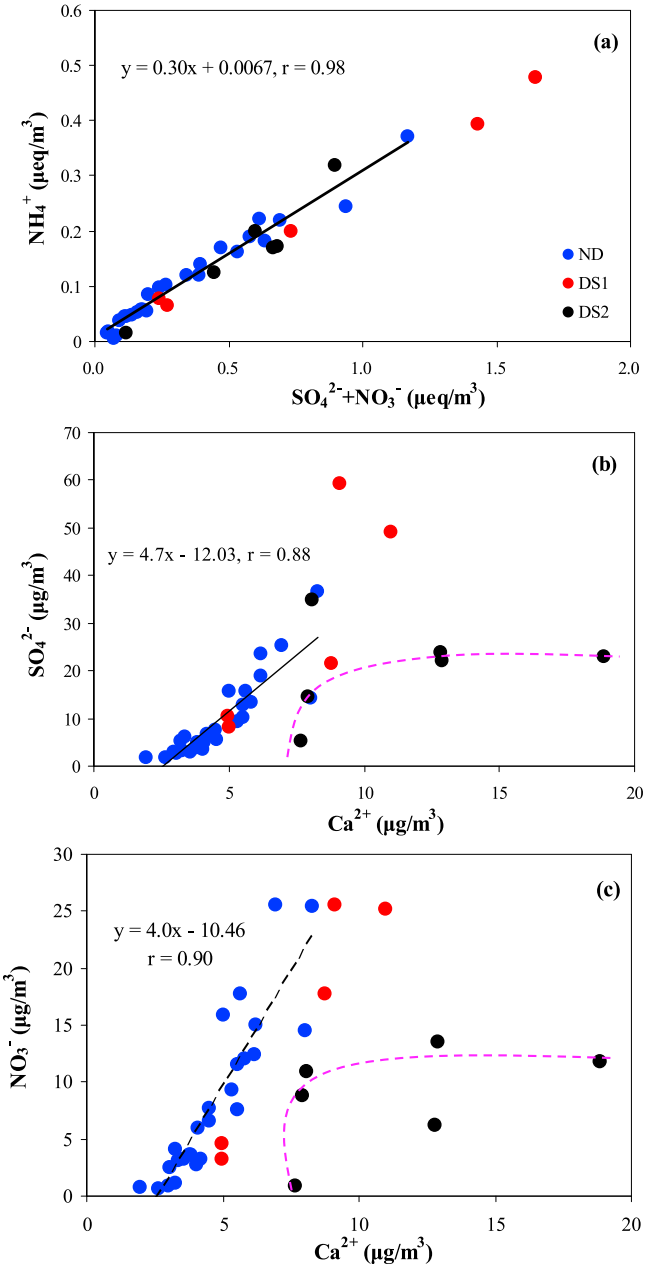

Figure 8. The relationship between (a) equivalent concentrations of NH_4^+ and sum of SO_4^{2-} and NO_3^-, (b) Ca^{2+} and SO_4^{2-}, and (c) Ca^{2+} and NO_3^- in TSP during ND, DS1 and DS2. Liner fits between two variables are only plotted for ND and the dashed line is for visual reference.

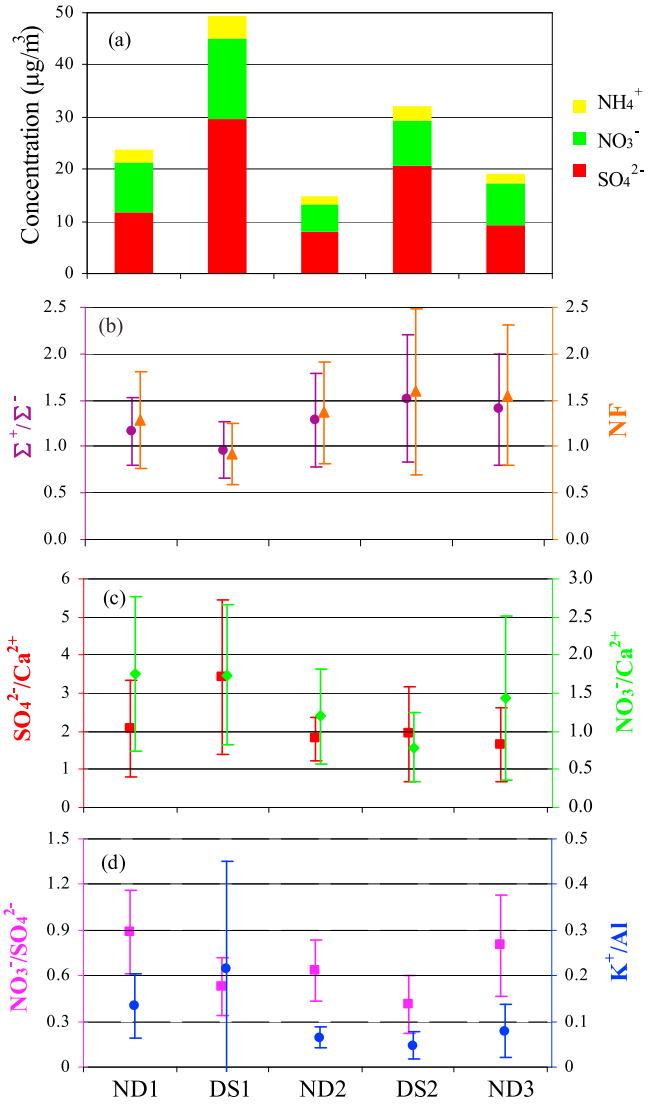

Figure 9. (a) The average mass concentrations of SO_4^{2-}, NO_3^- and NH_4^+. (b) The average ratios of $\sum^+/\sum^-$ and NF. (c) The average mass ratios of SO_4^{2-}/Ca^{2+} and NO_3^-/Ca^{2+}. (d) The average mass ratios of NO_3^-/SO_4^{2-} and K^+/Al during the two dust periods (i.e., DS1 and DS2) and three non-dust periods (i.e., ND1, ND2 and ND3). The error bars represent one standard deviation during each period. $\sum^+/\sum^-$ is defined as the ratio of the total equivalent cations to the total equivalent anions and NF is defined as the neutralization factor calculated as $(Ca^{2+} + NH_4^+)/(SO_4^{2-} + NO_3^-)$.

carbonate ($CaCO_3$), which played an important role in neutralizing the acids, and we found in this study that Ca^{2+} was the most abundant cation. The equivalent ratio of $(Ca^{2+} + NH_4^+)/(SO_4^{2-} + NO_3^-)$ was calculated and the average value was 1.40, 0.92 and 1.60 in ND, DS1 and DS2, respectively. This indicated that Ca^{2+} played a more important role in the neutralization process than NH_4^+ as the acids had almost been fully neutralized. The relationship of Ca^{2+} with SO_4^{2-} and NO_3^- in TSP is plotted in Figures 8b and 8c, respectively. Obviously, good correlations were observed between Ca^{2+} and SO_4^{2-} and between Ca^{2+} and NO_3^- in ND with correlation coefficients of 0.88 and 0.89, respectively. If the DS1 data (red dots) were included to the regression, good correlations could still be kept with correlation coefficients of 0.88 and 0.90, respectively. We also analyzed the correlation among the same species above in the fine $PM_{2.5}$ particles and found almost no significant correlation existed (correlation coefficient, $r < 0.1$), which suggested that coarse sulfate and nitrate were strongly influenced by the presence of calcium. Anyway, the situation was quite different for DS2. There was no such strong positive correlation between the variables as visualized by the dashed line in Figure 8, although this didn't preclude an influence of calcium on the formation of sulfate and nitrate. In DS1, due to the possible regional transport and high local gas concentrations of SO_2 and NO_2 with favorable meteorological conditions, such as moderate/high relative humidity and relatively low wind speed, the extent of the heterogeneous reaction between the pollution gases and mineral dust was assumed to be sufficient. In this regard, the DS1 plume could be considered as a pollution-dust well mixed event. In the case of DS2 displayed by the black dots in Figure 8, when the concentrations of calcium reached a certain value ($>10\mu g/m^3$), the concentrations of sulfate and nitrate tended to remain at a constant level, instead of increase, as it was in DS1. This would indicate that the formation of sulfate and nitrate was limited by the concentrations of gaseous precursors (SO_2, NO_2). As DS2 traveled over relatively clean regions, it had fewer chances to mix well with pollution precursors on the pathway, so the mixing extent was much lower than that of DS1.

[21] In order to better illustrate the evolution of aerosol composition during the sampling period, five periods were defined (The period before DS1, between DS1 and DS2, and after DS2 were defined as ND1, ND2 and ND3, respectively.). The average mass concentrations of SO_4^{2-}, NO_3^- and NH_4^+ in the five periods are presented in Figure 9a and all followed the sequence of DS1 > DS2 > ND1 > ND3 > ND2. As indicated above, the higher concentrations of the secondary species in dust plumes than those in the non-dust days were mainly attributed to the heterogeneous reaction and mixing of dust with pollution aerosol. We found that the interval period between the two dust events, which was defined as ND2, and the period after DS2, which was defined as ND3 had relatively low concentrations of pollution ions. That meant the two dust events were both followed by a relative clean atmospheric period and this was different from the previous studies in Beijing dust storm, when the pollutants, such as sulfate and nitrate, were observed to have a dramatic increase after the dust storms due to the formation of secondary ions on the suspended crustal particles remained in the atmosphere after the dust storm [*Wang et al.*, 2005]. This situation was probably related to the meteorological conditions. On April 12 and 19, which were the days after the dust plumes passed, the wind reached high speeds of 8.1 and 7.5 m/s, respectively, and the relatively humidity decreased to about 20%. The high wind speed facilitated the diffusion of pollutants and the low humidity was not favored the chemical transformation.

[22] Several tracers were used to explore more into the atmospheric processes in the above five periods (Figures 9b–9d). $\sum^+/\sum^-$ is designated to be the ratio of the total equivalent cations to the total equivalent anions. The ratio larger than 1.0 indicated the anion deficiency which was probably due to

Table 3. Correlation Coefficients Between AOD and Major Chemical Compositions in $PM_{2.5}$ and TSP[a]

$PM_{2.5}$	AOD (Fine)[b]	TSP	AOD (Total)[c]
BC	0.62	BC	0.57
SO_4^{2-}	0.73	SO_4^{2-}	0.46
NO_3^-	0.62	NO_3^-	0.34
NH_4^+	0.75	NH_4^+	0.38
K^+	0.76	K^+	0.47
TWSII	0.72	TWSII	0.49
Mineral	−0.19	Mineral	0.66

[a]BC, black carbon; TWSII, total water soluble inorganic ions; mineral, mineral aerosol.
[b]Fine model AOD.
[c]Total AOD.

the presence of CO_3^{2-}, as carbonate was unable to be measured by the ion chromatography used in this study, while the ratio less than 1.0 indicated the cation deficiency, as H^+ was not accounted for the total cations. The $\sum^+/\sum^-$ values averaged to be 1.17, 0.96, 1.29, 1.52 and 1.40 in the five periods, respectively. This result indicated that the alkalinity in DS2 was much higher than that in the other periods while the alkalinity of aerosol in DS1 was even lower than that in the non-dust days. This situation could be also verified by the NF (Neutralization Factor) tracer. NF is defined as the neutralization ability of bases on the acids in aerosol, which was calculated by using the formula $NF = (Ca^{2+} + NH_4^+)/(SO_4^{2-} + NO_3^-)$, in which the ions were equivalent mass concentrations. Higher NF values indicated the stronger neutralization ability, and vice versa. DS1 had the lowest value while DS2 had the highest among the five periods (Figure 9b). This was mainly attributed to the high production of acidic pollutions (mainly as SO_4^{2-} and NO_3^-) in DS1 as mentioned above. These results indicated that the aerosol of DS1 was the most acidic and that of DS2 was the most alkaline. The mass ratios of SO_4^{2-}/Ca^{2+} and NO_3^-/Ca^{2+} could be used to evaluate the extent of the heterogeneous reaction of SO_2/NOx on the surface of dust particles containing Ca (mainly as $CaCO_3$) (Figure 9c). SO_4^{2-}/Ca^{2+} ratio was highest in DS1, indicating the formation of sulfate was most favored during this period. The ratio in DS2 was close to that in the non-dust days but much lower than in DS1, indicating the mixing extent of SO_2 or sulfate with dust in DS1was much stronger than that in DS2. However, it was different in the case of nitrate. The NO_3^-/Ca^{2+} ratio didn't present an obvious peak in DS1 and it was the lowest in DS2 (Figure 9c), indicating the formation of nitrate was not enhanced during dust period as highly as sulfate. The different behaviors of formation of sulfate and nitrate could also be reflected by the variations of the ratio of NO_3^-/SO_4^{2-} (Figure 9d). The values in the dust periods (DS1 and DS2) were much lower than those in the other three non-dust periods, indicating the formation of sulfate was more favored than that of nitrate during the long-range transport of dust, although sulfate and nitrate both increased. The K^+/Al ratio could be used to evaluate the variation of biomass burning source (Figure 9d), as K^+ is the tracer for biomass burning and Al is the reference element of mineral source. Apparently, K^+/Al had the highest value during DS1, which was consistent with the previous discussion that DS1 was probably influenced by the biomass burning emission. In summary, the transport pathway of dust, the concentration of pollutant precursors, and the meteorological condition were the main factors affecting the mixing extent of pollutants with dust.

3.3. Relationship Between Chemical Species and AOD

[23] To find the major contributors to the aerosol optical depth (AOD) in the spring dust season, the relationship between AOD at 675nm and major aerosol chemical species were studied. As for the fine particles, fine mode aerosol optical depths were used to correlate with the $PM_{2.5}$ chemical species. The correlation coefficients are listed in Table 3. TWSII (Total Water Soluble Inorganic Ions) was defined as the total water soluble inorganic ions which was calculated by summing up all the inorganic ions, and mineral aerosol was calculated by using the formula [Mineral] = 2.2[Al] + 2.49[Si] + 1.63[Ca] + 2.42[Fe] + 1.94[Ti] [*Malm et al.*, 1994], where the concentration of Si was estimated using the crustal Si/Al ratio of 3.43. The major ionic species in $PM_{2.5}$, such as SO_4^{2-}, NO_3^- and NH_4^+, all had good correlations with fine mode AOD with the correlation coefficients of 0.73, 0.62, and 0.75, respectively (Figure 10). Besides, K^+ also had strong correlation with AOD with the correlation coefficient of 0.76 (Table 3). *Maring et al.* [2000] ever found that soluble K^+ was strongly correlated with total scattering during both dusty and non-dusty periods at Canary Islands. This indicated that anthropogenic aerosol such as sulfate, nitrate, ammonium, and smoke aerosol probably contributed much to the fine mode AOD. We compared the contribution of TWSII and mineral aerosol to the fine mode AOD and found that TWSII correlated well with AOD, while mineral aerosol almost had no correlation with it (Table 3). In addition, black carbon (BC) had a moderate correlation with AOD although BC only contributed an average of 2.9% to $PM_{2.5}$. *Lee et al.* [2009] concluded that 9–20% mass fraction of elemental carbon in aerosol could contribute up to 33–55% of particle light extinction in Seoul, indicating black carbon had a high extinction efficiency on aerosol light extinction. As a whole, the soluble ions and black carbon in the fine particles ($PM_{2.5}$) were the major contributors to fine mode AOD.

[24] As for the coarse particles, we used the total AOD at 675 nm and chemical species in TSP to analyze their relationship, and the result was totally different from that of fine particles. The major ions, such as SO_4^{2-}, NO_3^-, NH_4^+, and K^+ as well as TWSII, all had weak correlations with AOD (Table 3), indicating the contribution of soluble ions to AOD was not significant in coarse particles. Inversely, the mineral aerosol had good correlation with total AOD with the correlation coefficient of 0.66. In this study, the mineral aerosol contributed an average of (69.4 ± 13.6)% to total suspended particles. Although the extinction efficiency of dust was lower than that of soluble ions [*Lee et al.*, 2009], the dominant proportion of mineral aerosol over soluble ions would have overwhelmed the effect of soluble ions on the light extinction. *Cheng et al.* [2008] also found the typical mineral elements, such as Si, Fe, Ti, K etc., showed a strong correlation with AOD in dusty days over Beijing from 2004 to 2006. Moderate correlation between BC and AOD was still observed in coarse particles (Table 3), indicating black carbon contributed to AOD in both fine and coarse particles.

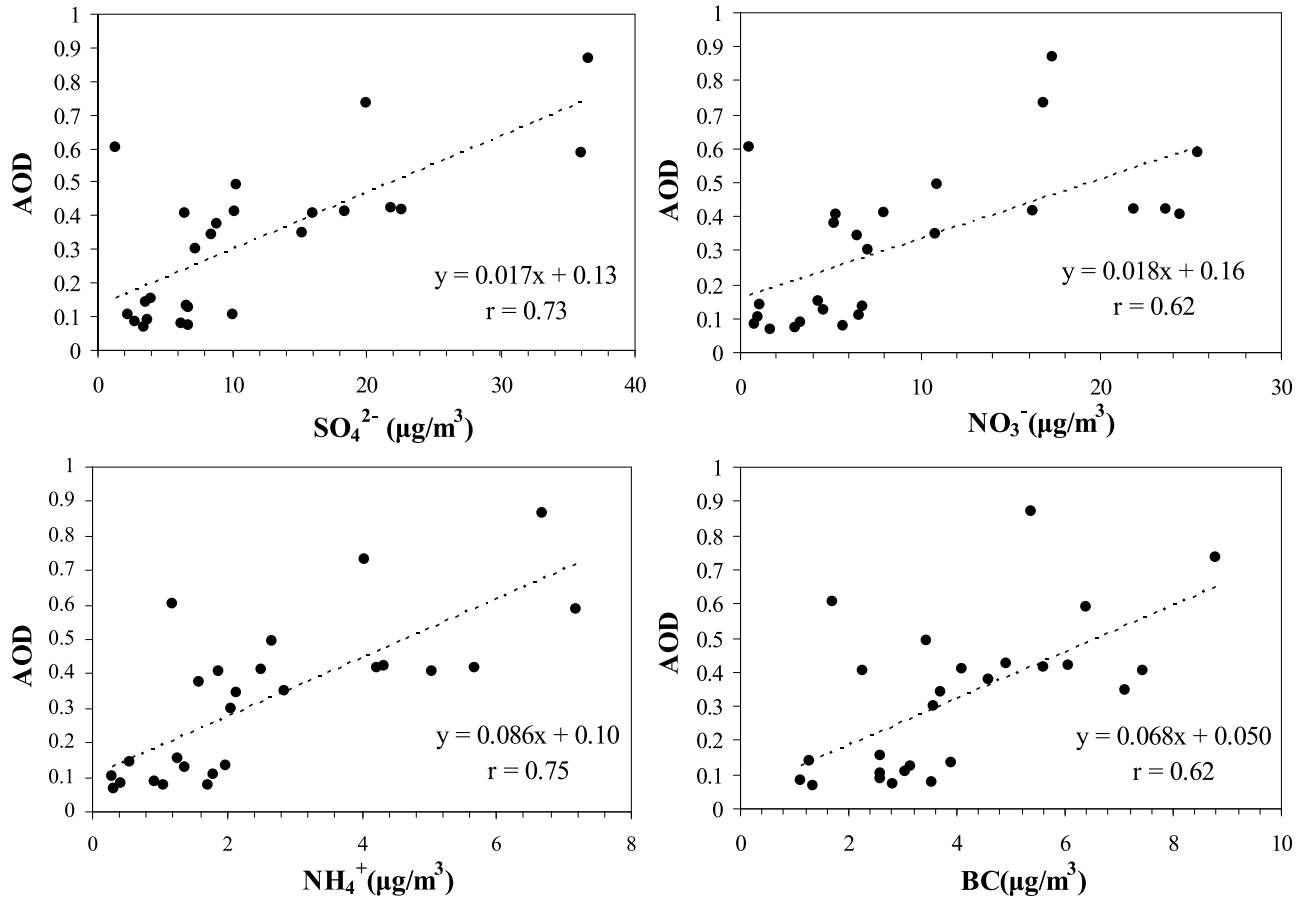

Figure 10. Correlations between AOD (fine mode) at 675nm and $PM_{2.5}$ species SO_4^{2-}, NO_3^-, NH_4^+ and black carbon (BC) during the spring dust season over Beijing in 2006.

[25] *Che et al.* [2009] found that the correlation of aerosol chemical composition with AOD was weak in three background stations in China. However, we link the aerosol optical properties well with its chemical composition in this study, although aerosol optical properties measured by Sun photometer represents the aerosol extinction in the atmospheric column, while the measured aerosol chemical composition are limited near the surface layer of atmosphere. This is probably due to the well mixed boundary layer in the spring dusty season and the extended vertical distribution of aerosol in the atmosphere. Our unpublished lidar data in the dust period indicated that the vertical distribution of extinction coefficients of the secondary aerosol was almost even during most of the dust periods, which means that the boundary layer was relatively well mixed. Although such data were not from the same sampling site and same sampling period as this study, the assumption of the boundary layer in the dust events is well mixed is reasonable to be applied in this study. The linear relationship between optical properties of column aerosol and chemical composition of ground aerosol suggested retrieval algorithms could be established to derive the ground aerosol information from the column aerosol optical measurements of satellite, and the relation between optical and chemical properties of dust aerosol could be established. Furthermore, the chemical composition of aerosol could be used to reflect their influence on the aerosol scattering, absorbing, and extinction properties and finally the radiative forcing.

4. Conclusions

[26] In order to evaluate the effect of long-range transport of dust on aerosol physicochemical properties, an aerosol sampling campaign consisting of $PM_{2.5}$ and TSP was conducted in Beijing from March 28th to April 28th in spring, 2006. Chemical composition, including elements, soluble ions, and black carbon were measured, and the aerosol optical properties were obtained from the AERONET Beijing site. Two dust plumes were identified, one from April 8th to April 11th and the other from April 17th to April 18th. The intensity of the second dust storm (DS2) was relatively higher and influenced larger area than the first one (DS1). The average TSP concentration of DS2 reached 683.3 $\mu g/m^3$, which corresponded to the extremely high AOD (440 nm) of 3.65 and the low Angstrom exponent of less than 0.2. Compared to DS2, DS1 had lower AOD and larger Angstrom exponent. The single scattering albedo (SSA) followed the order of ND > DS1 > DS2 at wavelength of 657, 870 and 1020 nm, as the percentage of black carbon in aerosol was the highest in ND compared to that in DS1 and DS2. Dust aerosol had strong light absorbing at 439 nm, and this was due to the significant proportion of iron oxides in the dust aerosol instead of black carbon. Enrichment factor (EF)

analysis indicated that pollution elements, i.e., Zn, As, Pb, S, and Cd, in DS1 were more enriched (EF > 100) than in DS2 and even in ND. Secondary ions, such as sulfate, nitrate, and ammonium were elevated about 2~3 times during DS1 compared to ND, indicating the strong heterogeneous chemical reaction occurred on the surface of dust and/or the mixing of dust with pollutant aerosol during the long-range transport of dust plumes. A significant increase of K^+ during DS1 also suggested the mixing of smoke aerosol with dust, which was confirmed by the MODIS fire spots from satellite. The mixing effect in DS2 was not as strong as that in DS1, which was mainly due to the different transport pathways of dust, as the air masses within the planetary boundary layer in DS1 passed through some industrial and urban regions. Generally, the transport pathways of dust, concentrations of pollutant precursors, and meteorological conditions were the main factors affecting the mixing extent of pollutants with dust. Linear relationship between aerosol optical properties and aerosol chemical compositions was found. This evaluation indicated that soluble ions, i.e., SO_4^{2-}, NO_3^-, NH_4^+, and K^+, were the main contributors to the light extinction of fine particles, while mineral aerosol contributed more to that of coarse particles. Black carbon, as a strong light absorbing species, was found to contribute to the light extinction of both fine and coarse particles.

[27] **Acknowledgments.** This work was supported by the National Key Project of Basic Research of China (grant 2006CB403704) and National Natural Science Foundation of China (grants 20877020, 20977017, and 40575062).We also thank the principal investigators of the AERONET Beijing site, Hongbin Chen and Philippe Goloub, for establishing and maintaining this site.

References

Alfaro, S. C., S. Lafon, J. L. Rajot, P. Formenti, A. Gaudichet, and M. Maillé (2004), Iron oxides and light absorption by pure desert dust: An experimental study, *J. Geophys. Res.*, *109*, D08208, doi:10.1029/2003JD004374.

Anderson, T. L., S. J. Masonis, D. S. Covert, N. C. Ahlquist, S. G. Howell, A. D. Clarke, and C. S. McNaughton (2003), Variability of aerosol optical properties derived from in situ aircraft measurements during ACE-Asia, *J. Geophys. Res.*, *108*(D23), 8647, doi:10.1029/2002JD003247.

Arimoto, R., W. Balsam, and C. Schloesslin (2002), Visible spectroscopy of aerosol particles collected on filters: Iron-oxide minerals, *Atmos. Environ.*, *36*, 89–96, doi:10.1016/S1352-2310(01)00465-4.

Bergstrom, R. W., P. Pilewskie, B. Schmid, and P. B. Russell (2003), Estimates of the spectral aerosol single scattering albedo and aerosol radiative effects during SAFARI 2000, *J. Geophys. Res.*, *108*(D13), 8474, doi:10.1029/2002JD002435.

Che, H., G. Shi, A. Uchiyama, A. Yamazaki, H. Chen, P. Goloub, and X. Zhang (2008), Intercomparison between aerosol optical properties by a PREDE skyradiometer and CIMEL sunphotometer over Beijing, China, *Atmos. Chem. Phys.*, *8*, 3199–3214, doi:10.5194/acp-8-3199-2008.

Che, H., Z. Yang, X. Zhang, C. Zhu, Q. Ma, H. Zhou, and P. Wang (2009), Study on the aerosol optical properties and their relationship with aerosol chemical compositions over three regional background stations in China, *Atmos. Environ.*, *43*, 1093–1099, doi:10.1016/j.atmosenv.2008.11.010.

Cheng, T., R. Zhang, Z. Han, and W. Fang (2008), Relationship between ground-based particle component and column aerosol optical property in dusty days over Beijing, *Geophys. Res. Lett.*, *35*, L20808, doi:10.1029/2008GL035284.

Davis, B. L., and G. Jixiang (2000), Airborne particulate study in five cities of China, *Atmos. Environ.*, *34*, 2703–2711, doi:10.1016/S1352-2310(99)00528-2.

Deaton, B. C., and W. L. Balsam (1991), Visible spectroscopy: A rapid method for determining hematite and goethite concentration in geological-materials, *J. Sediment. Petrol.*, *61*, 628–632.

Dubovik, O., and M. D. King (2000), A flexible inversion algorithm for retrieval of aerosol optical properties from Sun and sky radiance measurements, *J. Geophys. Res.*, *105*(D16), 20,673–20,696, doi:10.1029/2000JD900282.

Dubovik, O., B. Holben, T. F. Eck, A. Smirnov, Y. J. Kaufman, M. D. King, D. Tanre, and I. Slutsker (2002), Variability of absorption and optical properties of key aerosol types observed in worldwide locations, *J. Atmos. Sci.*, *59*, 590–608, doi:10.1175/1520-0469(2002)059<0590:VOAAOP>2.0.CO;2.

Eck, T. F., et al. (2005), Columnar aerosol optical properties at AERONET sites in central eastern Asia and aerosol transport to the tropical mid-Pacific, *J. Geophys. Res.*, *110*, D06202, doi:10.1029/2004JD005274.

Feng, J. L., L. P. Zhu, J. T. Ju, L. P. Zhou, X. L. Zhen, W. Zhang, and S. P. Gao (2008), Heavy dust fall in Beijing, on April 16–17, 2006: Geochemical properties and indications of the dust provenance, *Geochem. J.*, *42*, 221–236.

Fu, Q. Y., G. S. Zhuang, J. Wang, C. Xu, K. Huang, J. Li, B. Hou, T. Lu, and D. G. Streets (2008), Mechanism of formation of the heaviest pollution episode ever recorded in the Yangtze River Delta, China, *Atmos. Environ.*, *42*, 2023–2036, doi:10.1016/j.atmosenv.2007.12.002.

Guo, J., K. A. Rahn, and G. S. Zhuang (2004), A mechanism for the increase of pollution elements in dust storms in Beijing, *Atmos. Environ.*, *38*, 855–862, doi:10.1016/j.atmosenv.2003.10.037.

Holben, B. N., et al. (1998), AERONET: A federated instrument network and data archive for aerosol characterization, *Remote Sens. Environ.*, *66*, 1–16, doi:10.1016/S0034-4257(98)00031-5.

Huang, K., G. Zhuang, J. Li, Q. Wang, Y. Sun, Y. Lin, and J. S. Fu (2010), Mixing of Asian dust with pollution aerosol and the transformation of aerosol components during the dust storm over China in spring 2007, *J. Geophys. Res.*, *115*, D00K13, doi:10.1029/2009JD013145.

Huebert, B. J., T. Bates, P. B. Russell, G. Shi, Y. J. Kim, K. Kawamura, G. Carmichael, and T. Nakajima (2003), An overview of ACE-Asia: Strategies for quantifying the relationships between Asian aerosols and their climatic impacts, *J. Geophys. Res.*, *108*(D23), 8633, doi:10.1029/2003JD003550.

Kirchstetter, T. W., T. Novakov, and P. V. Hobbs (2004), Evidence that the spectral dependence of light absorption by aerosols is affected by organic carbon, *J. Geophys. Res.*, *109*, D21208, doi:10.1029/2004JD004999.

Liu, H., R. T. Pinker, M. Chin, B. Holben, and L. Remer (2008), Synthesis of information on aerosol optical properties, *J. Geophys. Res.*, *113*, D07206, doi:10.1029/2007JD008735.

Lee, S., Y. S. Ghim, S. W. Kim, and S. C. Yoon (2009), Seasonal characteristics of chemically apportioned aerosol optical properties at Seoul and Gosan, Korea, *Atmos. Environ.*, *43*, 1320–1328, doi:10.1016/j.atmosenv.2008.11.044.

Lee, Y. G., and C. H. Cho (2007), Characteristics of aerosol size distribution for a severe Asian dust event observed at Anmyeon, Korea in April 2006, *J. Korean Meteorol. Soc.*, *43*, 87–96.

Malm, W. C., J. F. Sisler, D. Huffman, R. A. Eldred, and T. A. Cahill (1994), Spatial and seasonal trends in particle concentration and optical extinction in the United States, *J. Geophys. Res.*, *99*(D1), 1347–1370, doi:10.1029/93JD02916.

Maring, H., D. L. Savoie, M. A. Izaguirre, C. McCormick, R. Arimoto, J. M. Prospero, and C. Pilinis (2000), Aerosol physical and optical properties and their relationship to aerosol composition in the free troposphere at Izaña, Tenerife, Canary Islands, during July 1995, *J. Geophys. Res.*, *105*(D11), 14,677–14,700, doi:10.1029/2000JD900106.

McKendry, I. G., A. M. Macdonald, W. R. Leaitch, A. van Donkelaar, Q. Zhang, T. Duck, and R. V. Martin (2008), Trans-Pacific dust events observed at Whistler, British Columbia during INTEX-B, *Atmos. Chem. Phys.*, *8*, 6297–6307, doi:10.5194/acp-8-6297-2008.

Mikami, M., et al. (2006), Aeolian dust experiment on climate impact: An overview of Japan-China joint project ADEC, *Global Planet. Change*, *52*, 142–172, doi:10.1016/j.gloplacha.2006.03.001.

Murayama, T., D. Müller, K. Wada, A. Shimizu, M. Sekiguchi, and T. Tsukamoto (2004), Characterization of Asian dust and Siberian smoke with multi-wavelength Raman lidar over Tokyo, Japan in spring 2003, *Geophys. Res. Lett.*, *31*, L23103, doi:10.1029/2004GL021105.

Myhre, G., C. R. Hoyle, T. F. Berglen, B. T. Johnson, and J. M. Haywood (2008), Modeling of the solar radiative impact of biomass burning aerosols during the Dust and Biomass-burning Experiment (DABEX), *J. Geophys. Res.*, *113*, D00C16, doi:10.1029/2008JD009857.

Nakajima, T., et al. (2007), Overview of the Atmospheric Brown Cloud East Asian Regional Experiment 2005 and a study of the aerosol direct radiative forcing in East Asia, *J. Geophys. Res.*, *112*, D24S91, doi:10.1029/2007JD009009.

Nishikawa, M., S. Kanamori, N. Kanamori, and T. Mizoguchi (1991), Kosa aerosol as eolian carrier of anthropogenic material, *Sci. Total Environ.*, *107*, 13–27, doi:10.1016/0048-9697(91)90247-C.

Noh, Y. M., D. Muller, D. H. Shin, H. Lee, J. S. Jung, K. H. Lee, M. Cribb, Z. Q. Li, and Y. J. Kim (2009), Optical and microphysical properties of

severe haze and smoke aerosol measured by integrated remote sensing techniques in Gwangju, Korea, *Atmos. Environ.*, *43*, 879–888, doi:10.1016/j.atmosenv.2008.10.058.

Papayannis, A., et al. (2007), Extraordinary dust event over Beijing, China, during April 2006: Lidar, Sun photometric, satellite observations and model validation, *Geophys. Res. Lett.*, *34*, L07806, doi:10.1029/2006GL029125.

Raut, J. C., P. Chazette, and A. Fortain (2009), Link between aerosol optical, microphysical and chemical measurements in an underground railway station in Paris, *Atmos. Environ.*, *43*, 860–868, doi:10.1016/j.atmosenv.2008.10.038.

Shi, Z., L. Shao, T. P. Jones, and S. Lu (2005), Microscopy and mineralogy of airborne particles collected during severe dust storm episodes in Beijing, China, *J. Geophys. Res.*, *110*, D01303, doi:10.1029/2004JD005073.

Shimizu, A., N. Sugimoto, I. Matsui, K. Arao, I. Uno, T. Murayama, N. Kagawa, K. Aoki, A. Uchiyama, and A. Yamazaki (2004), Continuous observations of Asian dust and other aerosols by polarization lidars in China and Japan during ACE-Asia, *J. Geophys. Res.*, *109*, D19S17, doi:10.1029/2002JD003253.

Sun, J. H., and L. N. Zhao (2008), Numerical simulation of two East Asian dust storms in spring 2006, *Earth Surf. Processes Landforms*, 33, 1892–1911, doi:10.1002/esp.1734.

Sun, Y., G. Zhuang, W. Ying, L. Han, J. Guo, D. Mo, W. Zhang, Z. Wang, and Z. Hao (2004), The air-borne particulate pollution in Beijing: Concentration, composition, distribution and sources, *Atmos. Environ.*, *38*, 5991–6004, doi:10.1016/j.atmosenv.2004.07.009.

Sun, Y., G. Zhuang, Y. Wang, X. Zhao, J. Li, Z. Wang, and Z. An (2005), Chemical composition of dust storms in Beijing and implications for the mixing of mineral aerosol with pollution aerosol on the pathway, *J. Geophys. Res.*, *110*, D24209, doi:10.1029/2005JD006054.

Wang, W., J. Z. Ma, S. Hatakeyama, X. Y. Liu, Y. Chen, A. Takami, L. H. Ren, and C. M. Geng (2008), Aircraft measurements of vertical ultrafine particles profiles over northern China coastal areas during dust storms in 2006, *Atmos. Environ.*, *42*, 5715–5720, doi:10.1016/j.atmosenv.2008.03.042.

Wang, Y., G. S. Zhuang, Y. Sun, and Z. S. An (2005), Water-soluble part of the aerosol in the dust storm season: Evidence of the mixing between mineral and pollution aerosols, *Atmos. Environ.*, *39*, 7020–7029, doi:10.1016/j.atmosenv.2005.08.005.

Wang, Y., G. S. Zhuang, A. H. Tang, W. J. Zhang, Y. L. Sun, Z. F. Wang, and Z. S. An (2007), The evolution of chemical components of aerosols at five monitoring sites of China during dust storms, *Atmos. Environ.*, *41*, 1091–1106, doi:10.1016/j.atmosenv.2006.09.015.

Xia, X. A., H. B. Chen, P. C. Wang, X. M. Zong, J. H. Qiu, and P. Gouloub (2005), Aerosol properties and their spatial and temporal variations over North China in spring 2001, *Tellus, Ser. B*, *57*, 28–39, doi:10.1111/j.1600-0889.2005.00126.x.

Xia, X. A., H. B. Chen, P. C. Wang, W. X. Zhang, P. Goloub, B. Chatenet, T. F. Eck, and B. N. Holben (2006), Variation of column-integrated aerosol properties in a Chinese urban region, *J. Geophys. Res.*, *111*, D05204, doi:10.1029/2005JD006203.

Xia, X., H. Chen, and W. Zhang (2007), Analysis of the dependence of column-integrated aerosol properties on long-range transport of air masses in Beijing, *Atmos. Environ.*, *41*, 7739–7750, doi:10.1016/j.atmosenv.2007.06.042.

Yuan, H., Y. Wang, and G. S. Zhuang (2003), Simultaneous determination of organic acids, methanesulfonic acid and inorganic anions in aerosol and precipitation samples by ion chromatography, *J. Instrum. Anal.*, *22*, 11–44.

Yuan, H., K. A. Rahn, and G. Zhuang (2004), Graphical techniques for interpreting the composition of individual aerosol particles, *Atmos. Environ.*, *38*, 6845–6854, doi:10.1016/j.atmosenv.2004.09.010.

Yuan, H., G. Zhuang, K. A. Rahn, X. Zhang, and Y. Li (2006), Composition and mixing of individual particles in dust and nondust conditions of North China, spring 2002, *J. Geophys. Res.*, *111*, D20208, doi:10.1029/2005JD006478.

Yuan, H., G. S. Zhuang, J. Li, Z. F. Wang, and J. Li (2008), Mixing of mineral with pollution aerosols in dust season in Beijing: Revealed by source apportionment study, *Atmos. Environ.*, *42*, 2141–2157, doi:10.1016/j.atmosenv.2007.11.048.

Zheng, Y., and S. H. Zhang (2008), Magnetic properties of street dust and topsoil in Beijing and its environmental implications, *Chin. Sci. Bull.*, *53*, 408–417, doi:10.1007/s11434-007-0450-3.

Zhuang, G., J. Guo, H. Yuan, and C. Zhao (2001), The compositions, sources, and size distribution of the dust storm from China in spring of 2000 and its impact on the global environment, *Chin. Sci. Bull.*, *46*, 895–900, doi:10.1007/BF02900460.

J. S. Fu, Department of Civil and Environmental Engineering, University of Tennessee, Knoxville, TN 37996, USA.

K. Huang, J. Li, Y. Lin, and G. Zhuang, Center for Atmospheric Chemistry Study, Department of Environmental Science and Engineering, Fudan University, Shanghai, 200433, China. (gzhuang@fudan.edu.cn)

Y. Sun, Department of Environmental Toxicology, University of California, Davis, CA 95616, USA.

W. Zhang, Chinese Research Academy of Environmental Sciences, Beijing, 100012, China.